THE JOURNAL OF BIOLOGICAL CHEMISTRY VOL. 287, NO. 39, pp. 32717–32727, September 21, 2012

Distinctive Features of Catalytic and Transport Mechanisms in Mammalian Sarco-endoplasmic Reticulum Ca^{2+} ATPase (SERCA) and Cu^{+} (ATP7A/B) ATPases*

Received for publication, April 18, 2012, and in revised form, July 26, 2012 Published, JBC Papers in Press, August 1, 2012, DOI 10.1074/jbc.M112.373472

David Lewis[‡], Rajendra Pilankatta[‡], Giuseppe Inesi[‡1], Gianluca Bartolommei[§], Maria Rosa Moncelli[§], and Francesco Tadini-Buoninsegni[§2]

From the [‡]California Pacific Medical Center Research Institute, San Francisco, California 94107 and the [§]Department of Chemistry "Ugo Schiff," University of Florence, 50019 Sesto Fiorentino, Italy

Background: SERCA and ATP7A/B are P-type ATPases entailing phosphoenzyme intermediate (E-P) formation.
Results: Biochemical characterization, however, reveals distinctive features.
Conclusion: A H^+-gated Ca^{2+} pathway coupled to E1-P to E2-P transition is SERCA-specific. Headpiece interactions with an *N*-metal binding extension (NMBD) and related conformational constraints are ATP7A/B-specific.
Significance: SERCA and ATP7A/B mechanisms present significant differences even though they are both P-type.

Ca^{2+} (sarco-endoplasmic reticulum Ca^{2+} ATPase (SERCA)) and Cu^{+} (ATP7A/B) ATPases utilize ATP through formation of a phosphoenzyme intermediate (E-P) whereby phosphorylation potential affects affinity and orientation of bound cation. SERCA E-P formation is rate-limited by enzyme activation by Ca^{2+}, demonstrated by the addition of ATP and Ca^{2+} to SERCA deprived of Ca^{2+} (E2) as compared with ATP to Ca^{2+}-activated enzyme ($E1{\cdot}2Ca^{2+}$). Activation by Ca^{2+} is slower at low pH ($2H^{+}{\cdot}E2$ to $E1{\cdot}2Ca^{2+}$) and little sensitive to temperature-dependent activation energy. On the other hand, subsequent (forward or reverse) phosphoenzyme processing is sensitive to activation energy, which relieves conformational constraints limiting Ca^{2+} translocation. A "H^{+}-gated pathway," demonstrated by experiments on pH variations, charge transfer, and Glu-309 mutation allows luminal Ca^{2+} release by H^{+}/Ca^{2+} exchange. As compared with SERCA, initial utilization of ATP by ATP7A/B is much slower and highly sensitive to temperature-dependent activation energy, suggesting conformational constraints of the headpiece domains. Contrary to SERCA, ATP7B phosphoenzyme cleavage shows much lower temperature dependence than *E*P formation. ATP-dependent charge transfer in ATP7A and -B is observed, with no variation of net charge upon pH changes and no evidence of Cu^{+}/H^{+} exchange. As opposed to SERCA after Ca^{2+} chelation, ATP7A/B does not undergo reverse phosphorylation with P_i after copper chelation unless a large *N*-metal binding extension segment is deleted. This is attributed to the inactivating interaction of the copper-deprived *N*-metal binding extension with the headpiece domains. We conclude that in addition to common (P-type) phosphoenzyme intermediate formation, SERCA and ATP7A/B possess distinctive features of catalytic and transport mechanisms.

Early studies of P-type ATPases (1–3) suggested a common mechanistic feature of cation transport based on an E1 to E2 conformational transition of the ATPase protein whereby affinity and orientation of cation binding sites are changed to promote vectorial translocation. This appears clearly in the Ca^{2+} ATPase, where the free energy of ATP is utilized to destabilize the $E1{\cdot}2Ca^{2+}$ state through formation of a phosphorylated intermediate that undergoes sequential processing as proposed in Scheme 1.

The Ca^{2+} ATPase (SERCA)[3] is a mammalian membrane-bound protein sustaining Ca^{2+} transport and involved in cell Ca^{2+} signaling and homeostasis (4). It is made of a single polypeptide chain of 994 amino acid residues (5) distributed in 10 transmembrane segments (M1–M10) and a cytosolic headpiece including three distinct domains (A, N, and P) that are directly involved in catalytic activity (Fig. 1). The N domain contains residues (such as Phe-487) interacting with the adenosine moiety of ATP whereby the ATP substrate is cross-linked to the P domain. The P domain contains a residue (Asp-351) undergoing phosphorylation to yield a phosphoenzyme intermediate, a residue (Asp-703) coordinating Mg^{2+}, and other features characteristic of P-type ATPases (6, 7). The A domain includes the signature sequence ^{181}TGES that provides catalytic assistance for final hydrolytic cleavage of phosphoenzyme (8–10). Cooperative and sequential binding (11) of two Ca^{2+} involved in catalytic activation and transport occur on sites (I and II) located within the transmembrane region rather close to the cytoplasmic surface of the lipid bilayer (12).

Interesting comparative questions relate to the mammalian copper ATPases ATP7A/B (13–15), which are also P-type ATPases but sustain active transport of copper by utilization of ATP and are involved in copper homeostasis (16–20). It is shown in Fig. 1 that the ATP7B (as well as ATP7A) isoform comprises eight (rather than 10) transmembrane segments

* This work was supported, in whole or in part, by National Institutes of Health Grant RO1 HL69830. This work was also supported by Ente Cassa di Risparmio di Firenze (2009.0749) and the Italian Ministry of Education, University and Research (PRIN Project 20083YM37E).
[1] To whom correspondence should be addressed. Tel.: 1-415-6001745; Fax: 1-415-6001725; E-mail: ginesi@cpmcri.com.
[2] To whom correspondence should be addressed. Tel.: 39-055-4573239; Fax: 39-055-4573142, E-mail: francesco.tadini@unifi.it.

[3] The abbreviations used are: SERCA, sarco-endoplasmic reticulum Ca^{2+} ATPase; SR, sarcoplasmic reticulum; ATP7A/B, Cu^{+} ATPases; SSM, solid supported membrane; BCS, bathocuproine disulfonate; NMBD, *N*-metal binding domain; TMBS, transmembrane binding site.

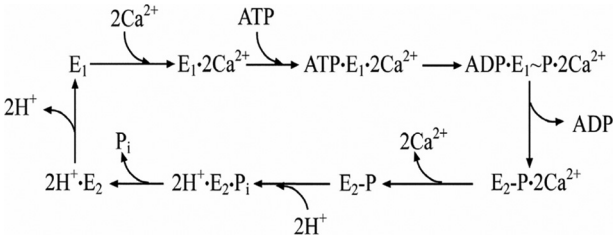

SCHEME 1.

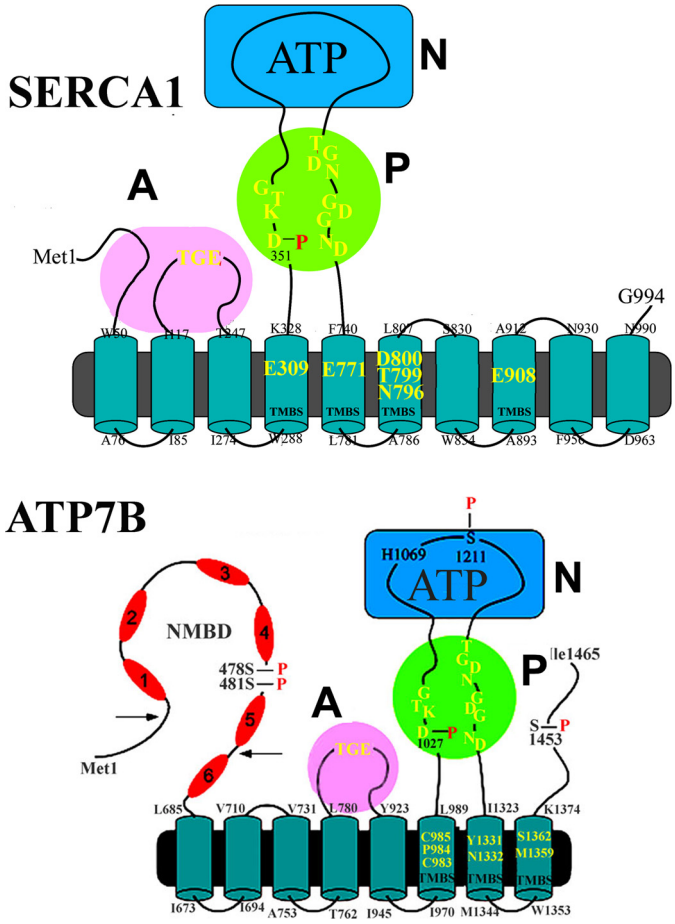

FIGURE 1. **Two-dimensional folding models of the SERCA (*upper panel*) and ATP7B (*lower panel*) sequences.** The diagrams show 10 (*SERCA*) or 8 (*ATP7B*) transmembrane segments including the calcium or copper binding sites (*TMBS*) involved in enzyme activation and transport. The extramembranous region of both enzymes comprises a nucleotide binding domain (*N*), the *P* domain, with several residues (in *yellow*) conserved in P-type ATPases, including the aspartate (Asp-351 or Asp-1027) that undergoes phosphorylation to form the catalytic phosphoenzyme intermediate (*EP*), and the A domain with the TGE conserved sequence involved in catalytic assistance of *EP* hydrolytic cleavage. The His-1069 residue whose mutation is frequently found in Wilson disease is shown on the N domain of ATP7B. Specific features of ATP7B are the *N*-metal binding domain (*NMBD*) extension with six putative copper binding sites and serine residues undergoing kinase-assisted phosphorylation (Ser-478, Ser-481, Ser-1211, Ser-1453).

including a copper binding site (TMBS) for catalytic activation and transport and a headpiece including the N, P, and A domains with conserved catalytic motifs analogous to SERCA. A specific feature of mammalian copper ATPases is an amino-terminal extension (NMBD) that includes six copper binding sites in addition to the TMBS (19). An additional feature is the presence of serine residues (Ser-478, Ser-481, Ser-1211, Ser-1453 in ATP7B) undergoing kinase-assisted phosphorylation (21).

Several analogies listed above suggest functional similarity in calcium and copper ATPases. However, we report here that experimental characterization of partial reactions reveals that even though both ATPases include P-type phosphoenzyme formation, the two enzymes present significant diversities in energy transduction, sequence of conformational transitions, and H^{+} involvement.

EXPERIMENTAL PROCEDURES

Protein Production and Biochemical Characterization—Native calcium ATPase (SERCA) was obtained with the microsomal fraction of rabbit skeletal muscle (22), which is referred to as sarcoplasmic reticulum (SR) vesicles. WT and mutant recombinant calcium (SERCA1) and copper ATPases (ATP7A and ATP7B) were obtained from COS1 cells infected with adenovirus vectors containing CMV promoter-driven cDNA fused with a 3′ c-Myc tag as described previously (21). The content of specific expressed protein was evaluated in the microsomal fraction of the infected COS1 cells by SDS gel electrophoresis and Western blotting (21).

Steady state ATPase hydrolytic activity was determined after P_i production by colorimetry (21). The reaction mixture contained 50 mM MES (pH 6.0) or HEPES (pH 7.5), 80 mM KCl (or as specified in figure legends), 3 mM $MgCl_2$, 0.2 mM EGTA, 0.2 mM $CaCl_2$, 30 μg of SR protein/ml, and 1 μM A23187 Ca^{2+} ionophore. The reaction was started by the addition of 2.5 mM ATP at 30 °C temperature.

[^{32}P]Phosphoenzyme formation was determined by incubating microsomes (50 μg of microsomal protein/ml) derived from rabbit skeletal muscle (native SERCA) with 50 μM [γ-^{32}P]ATP at 10 or 30 °C in a reaction mixture containing 50 mM MES (pH 6.0) or HEPES (pH 7.5), 80 mM KCl, 3 mM $MgCl_2$, and 20 μM $CaCl_2$ or otherwise as stated in figure legends. Substrate addition and quenching at serial times with 5% trichloroacetic acid were done on continuously vortexed reaction mixtures. The quenched samples were filtered through 0.45-μm Millipore nitrocellulose filters that were then washed 3 times with cold 0.125 M perchloric acid and once with water and processed for determination of radioactivity by scintillation counting.

In most cases, however, microsomes derived from COS-1 cells expressing WT or mutant SERCA (rather than muscle microsomes containing native SERCA) were used. The microsomes containing recombinant SERCA1 (50 μg of microsomal protein/ml) were incubated with 50 μM [γ-^{32}P]ATP at 10 or 30 °C in reaction mixtures analogous to those described above. Samples were quenched at serial times with 5% trichloroacetic acid. In this case, the quenched samples were pelleted by centrifugation at 5000 rpm for 5 min, washed with 0.125 N perchloric acid, and finally resuspended in pH 8.3 (half of the sample) or pH 6.3 loading buffer (remaining half of the sample) and separated by alkaline (23) or acid buffer (24) gel electrophoresis. The gels were dried and exposed to a phosphor screen followed by scanning on a Typhoon scanner (Amersham Biosciences) for stoichiometric determination of phosphoprotein relative to three [γ-^{32}P]ATP standards placed on the gels.

For characterization of copper ATPase, microsomes derived from COS-1 cells expressing recombinant enzyme were preincubated for 30 min in a medium containing 5.0 mM MES trieth-

anolamine (pH 6.0), 300 mM KCl, 10 mM DTT, 3 mM $MgCl_2$, and 5 μM $CuCl_2$. The low MES concentration facilitated pH changes if required by the experimental protocol.

Formation of [^{32}P]phosphoenzyme was obtained by incubating ATP7B (50 μg of microsomal protein/ml) with 50 μM [γ-^{32}P]ATP at 10 or 30 °C in a reaction mixture containing 50 mM MES triethanolamine (pH 6.0) or HEPES (pH 7.5), 300 mM KCl, 10 mM DTT, 3 mM $MgCl_2$, and 5 μM $CuCl_2$. The samples were quenched and processed for electrophoresis as explained above.

Decay of the phosphorylated enzyme intermediate in the forward direction of the catalytic cycle was determined by first reaching steady state levels of radioactive phosphoenzyme by incubation with [γ-^{32}P]ATP for 15 s at which time 1 mM non-radioactive ATP was added, and the samples were acid-quenched at various times. The quenched samples were dissolved in detergent at acidic or alkaline pH and separated by electrophoresis at acidic or alkaline pH for determination of residual phosphoenzyme.

For reverse phosphorylation with P_i, microsomes derived from muscle or microsomes derived from COS1 cells expressing SERCA or mutant proteins were incubated with 50 mM MES (pH 6.0) or HEPES (pH 7.5), 20% Me_2SO_4, 10 mM $MgCl_2$, and 2 mM EGTA. 100 mM KCl and 1 mM $CaCl_2$ (in the absence of EGTA) were added when indicated. The reaction was started by the addition of 50 μM [^{32}P]P_i, quenched at different times, and processed for determination of radioactive protein either on filters or electrophoresis as described for phosphorylation with ATP.

Charge Measurements—Charge movements were measured by adsorbing native SR vesicles containing SERCA or microsomes from COS-1 cells containing recombinant SERCA or Cu^+ ATPase (ATP7A or ATP7B) on a solid supported membrane (SSM). The SSM consists of an alkanethiol monolayer covalently bound to a gold electrode via the sulfur atom and a phospholipid monolayer on top of it (25). After adsorption, the protein (calcium or copper ATPase) was activated by a concentration jump of a suitable substrate, *i.e.* ATP, in the presence of buffer solutions of various compositions. If at least one electrogenic step is involved in the relaxation process after activation, a current transient can be recorded along the external circuit (26, 27). Numerical integration of each transient is related to a net charge movement that depends upon the particular electrogenic event. In addition, kinetic information can be obtained by fitting a sum of exponentially decaying terms to the current *versus* time curves.

In experiments with native or recombinant SERCA, the solution contained 100 mM choline chloride (or 100 mM KCl), 25 mM MOPS, pH 7.0, 1 mM $MgCl_2$, 0.25 mM EGTA, 0.25 mM $CaCl_2$ (10 μM free Ca^{2+}), and 0.2 mM DTT. Activation was obtained by the addition of ATP (100 μM) contained in a solution of the same composition. Free Ca^{2+} concentration was calculated with the computer program WinMAXC (28). Unless otherwise stated, 1 μM calcium ionophore A23187 was used to prevent formation of a Ca^{2+} concentration gradient across the SR vesicles (29). In ATP concentration-jump experiments with recombinant ATP7A or ATP7B, the non-activating solution contained 300 mM KCl (or 300 mM choline chloride), 50 mM MES triethanolamine, pH 6.0, 5.0 mM $MgCl_2$, 0.1 mM $CaCl_2$, 10 mM DTT, and 5 μM $CuCl_2$; the activating solution contained, in addition, 100 μM ATP.

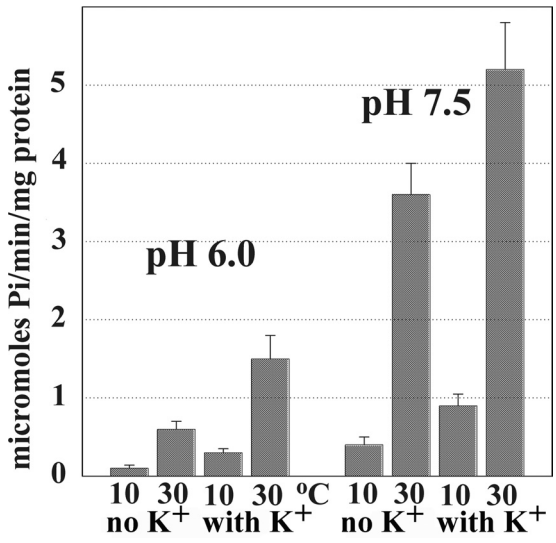

FIGURE 2. **Steady state Ca^{2+} ATPase activity of native Ca^{2+} ATPase.** ATP hydrolysis was measured at pH 6.0 or 7.5 in the presence of a Ca^{2+} ionophore (A23187) to prevent Ca^{2+} accumulation in SR vesicles and ATPase "back inhibition." The reaction mixture contained 50 mM MES (pH 6.0) or HEPES (pH 7.5), 80 mM KCl (when indicated), 3 mM $MgCl_2$, 20 μM $CaCl_2$, 30 μg of SR protein/ml, and 1 μM A23187. A low rate of Ca^{2+}-independent ATPase activity, measured in the presence of EGTA and no added Ca^{2+}, was subtracted from the total. The reaction was started by the addition of 2.5 mM ATP at 10 or 30 °C temperature, and samples were collected at time intervals. ATPase velocity was calculated from linear slopes of P_i production.

The concentration jump experiments were carried out by employing the SURFE^{2}R^{One} device (Scientific Devices Heidelberg, Germany). The temperature was maintained at 22–23 °C for all the experiments.

To verify the reproducibility of the current transients generated within the same set of measurements on the same SSM, each single measurement of the set was repeated six times and then averaged to improve the signal to noise ratio. Standard deviations were usually found to be no greater than ±5%. Moreover, each set of measurements was usually reproduced using 3–5 different SSM electrodes. Therefore, the data points reported in Fig. 5 represent the mean of 3–5 independent normalized values. S.E. are given by individual error bars in the figure.

RESULTS

Steady State Activity of Calcium Transport ATPase—The effects of pH, K^+, and temperature on the steady state ATP utilization by native SERCA (SR vesicles) are shown in Fig. 2. In these experiments a Ca^{2+} ionophore (30) was added to the reaction mixture to prevent Ca^{2+} accumulation and back inhibition of ATPase activity, thereby obtaining constant velocity of ATP consumption. It is clear that the overall turnover is dependent on the reaction temperature, which is consistent with a 22–25 kcal mol^{-1} energy of activation previously reported (31). Under all conditions, the ATPase velocity is significantly increased by the presence of K^+. Furthermore, the ATPase velocity is much higher when the pH is increased from 6.0 to 7.5, indicating a strong pH dependence of enzyme turn-

over. In contrast, it was previously found (in the absence of ionophore) that ATP-dependent Ca^{2+} load into SR vesicles is lower at alkaline than acid pH (29, 32).

Sequential Reactions of the SERCA Cycle—In early kinetic studies performed at 25 °C temperature and at neutral pH, we found that the addition of ATP to SERCA already activated with Ca^{2+} is followed by rapid phosphoenzyme formation, with a rate constant of ~100 s^{-1}, which was significantly slower if ATP and Ca^{2+} were added to enzyme deprived of Ca^{2+} (11). Here, as a base line to experiments on pH and temperature dependence of native and recombinant calcium and copper ATPases, we obtained measurements at pH 6.0 and 10 °C and found that even under these conditions phosphorylation after the addition of ATP and Ca^{2+} to enzyme deprived of Ca^{2+} is significantly slower than phosphorylation after the addition of ATP to enzyme preincubated with Ca^{2+} (Fig. 3*A*). This demonstrates that SERCA activation by Ca^{2+} requires a rate-limiting transition that is slower at acid than at alkaline pH (Fig. 3*B*). Therefore, activation by Ca^{2+} is easier if the enzyme resides in the state E1 rather than in the state $2H^{+}$·E2 (see Scheme 1 in the Introduction). Furthermore, we observed a requirement for ionic strength and a specific activation by K^{+} when we compared K^{+} to NH_4^{+} (not shown).

The initial velocity of SERCA activation by Ca^{2+} (required for ATP utilization) is approximately the same at low and high temperature (Fig. 3, *C* and *D*). On the other hand, a higher steady state level of phosphoenzyme is reached at lower temperature, suggesting significant temperature dependence of subsequent steps leading to hydrolytic cleavage of the phosphoenzyme. In fact, it is shown in Fig. 3, *E* and *F*, that decay of radioactive phosphoenzyme intermediate after a chase with excess nonradioactive ATP is clearly temperature-dependent and is favored by alkaline pH. Therefore, completion of enzyme turnover involves transitions of conformational states that are sensitive to temperature-dependent energy of activation, as also indicated by measurements of steady state ATPase velocity (Fig. 2).

ATP Utilization by Copper ATPase (ATP7B)—In comparative studies we examined the mammalian copper ATPase. Functional characterization of copper ATPases requires heterologous expression, as native sources are not sufficiently abundant. For this reason we used microsomes derived from COS-1 cells infected with adenovirus vector and expressing recombinant ATP7A/B (or SERCA for comparison).

When phosphoprotein formation by recombinant calcium and copper ATPases are compared, we find that ATP utilization by SERCA yields only autophosphorylation of a conserved aspartate serving as phosphoenzyme intermediate. On the other hand, ATP7B yields autophosphorylation of the conserved aspartate as well as kinase-assisted phosphorylation of serine residues (21). Aspartate and serine phosphorylation can be distinguished by running samples at acid and alkaline electrophoresis. Although alkali-resistant phosphoprotein is not obtained with SERCA (Fig. 4*A*), phosphorylation of ATP7B includes alkali resistant and alkali labile fractions (Fig. 4*B*). The difference between total and alkali resistant phosphoprotein (*i.e.* alkali labile) corresponds to aspartyl phosphate intermediate. Alkali labile phosphorylation of ATP7B does not occur

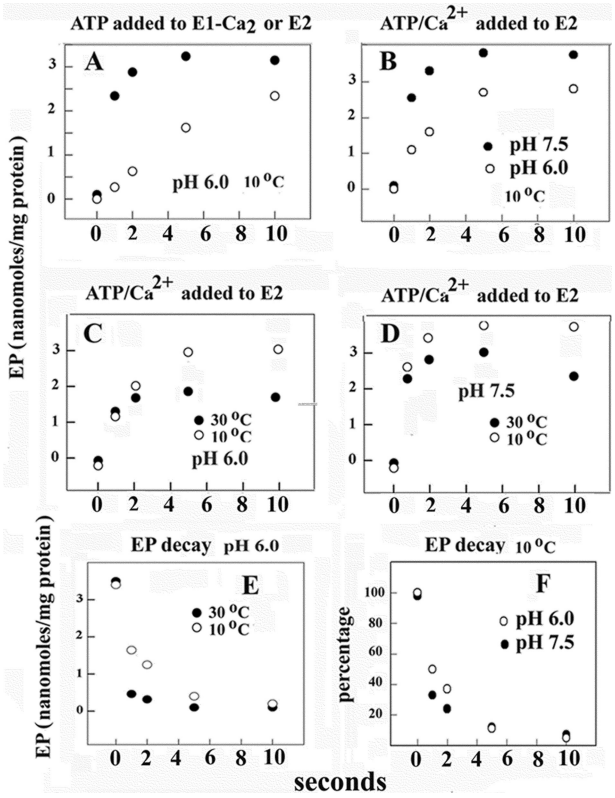

FIGURE 3. **Time course of phosphoenzyme intermediate formation (*A*, *B*, *C*, and *D*) after the addition of ATP to Ca^{2+} ATPase and subsequent phosphoenzyme decay (*E* and *F*).** Phosphorylation was obtained by the addition of 50 μM [γ-^{32}P]ATP to ATPase preincubated with Ca^{2+} (● in *A*) or the addition of 50 μM [γ-^{32}P]ATP and Ca^{2+} to ATPase deprived of Ca^{2+} (○ in *A* and all variables in *B–D*) at 10 or 30 °C as indicated. The reaction mixture contained 50 mM HEPES (pH 7.5) or 50 mM MES (pH 6.0), 80 mM KCl, and 3 mM $MgCl_2$. The $CaCl_2$ concentration was 20 μM in *A*. Alternatively, the reaction mixture contained 1 mM (at pH 7.5) or 5 mM EGTA (at pH 6.0) before the addition of ATP and then either 1 mM (at pH 7.5) or 5 mM (at pH 6.0) $CaCl_2$ was added with the [γ-^{32}P]ATP. The reaction was quenched at serial times with 5% trichloroacetic acid, and the quenched samples were filtered through 0.45-μm Millipore nitrocellulose filters that were then washed 3 times with cold 0.125 M perchloric acid and once with water and processed for determination of radioactivity by scintillation counting. Decay of phosphoenzyme intermediate (*E* and *F*) was obtained by first incubating ATPase with [γ-^{32}P]ATP for 10 s at pH 6 and 10 °C temperature followed by a 4-fold dilution with an identical medium but containing 1 mM nonradioactive ATP. Temperature and pH are as indicated in the figure. Quenching and collection of serial samples are as described above. The experimental points are averages of values obtained in three to four different experiments.

after mutations at the transmembrane copper binding site (33) and is, therefore, linked specifically to enzyme activation (E2 to E1 transition) by occupancy of the cation transport site. It is noteworthy that ATP7A undergoes aspartate phosphorylation with kinetics analogous to ATP7B, but a lower level of protein kinase assisted phosphorylation (34).

We now find that even though a copper binding requirement for the E2 to the E1 transition is demonstrated by copper site mutations (33), experiments analogous to those with SERCA, in which Ca^{2+} is first chelated with EGTA and then Ca^{2+} is added to produce activation, cannot be easily done with ATP7A/B. In fact copper chelation with BCS produces inactivation due to removal of copper from the NMBD in addition to the TMBS, and very low phosphoenzyme formation is then obtained after the addition of copper and ATP.

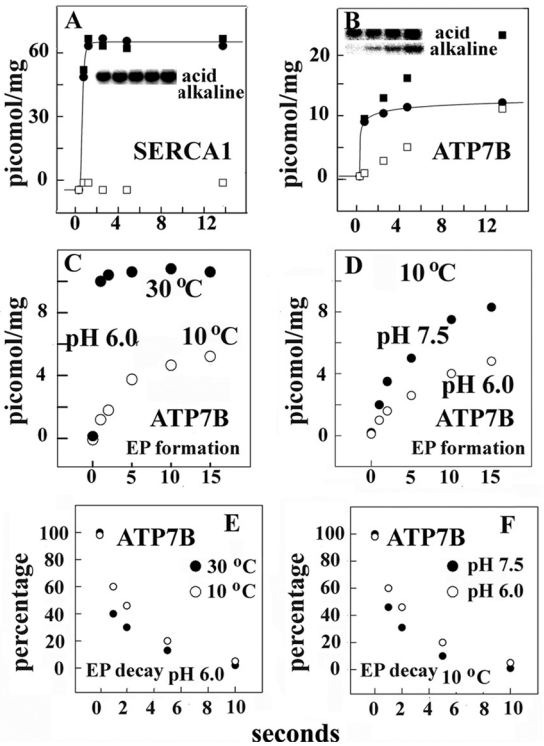

FIGURE 4. **Phosphoprotein formation after the addition of ATP to recombinant SERCA (*A*) or ATP7B (*B–D*) and subsequent decay of ATP7B phosphoenzyme (*E* and *F*).** Microsomes obtained from COS-1 cells sustaining heterologous expression were incubated with 50 μM [γ-^{32}P]ATP at 10 or 30 °C at various pH levels as explained under "Experimental Procedures." Electrophoresis in acid buffer or alkaline buffer was then performed to distinguish total [^{32}P]phosphoprotein (■) from alkali-resistant [^{32}P]phosphoprotein (serine and/or threonine, □). The difference is considered alkali-labile [^{32}P]phosphoprotein (aspartate, ●) and attributed to formation of phosphorylated enzyme intermediate. *acid* and *alkaline* refer to the media used for resuspension of samples and electrophoresis. Electrophoretic gel images correspond to sequential samples obtained within the time scale shown in the *horizontal axis*. Note that no alkaline-resistant phosphoprotein was obtained with SERCA, whereas both alkaline-resistant and alkaline-labile phosphorylation were obtained with ATP7B. Only the difference (phosphorylated enzyme intermediate) is shown in the *lower panels* (*C–F*). Decay of phosphoenzyme was measured as explained under "Experimental Procedures" and in the legend to Fig. 3. The experimental points are averages of values obtained in three to four different experiments. The electrophoretic images in *A* and *B* are examples of data repeated in all experiments.

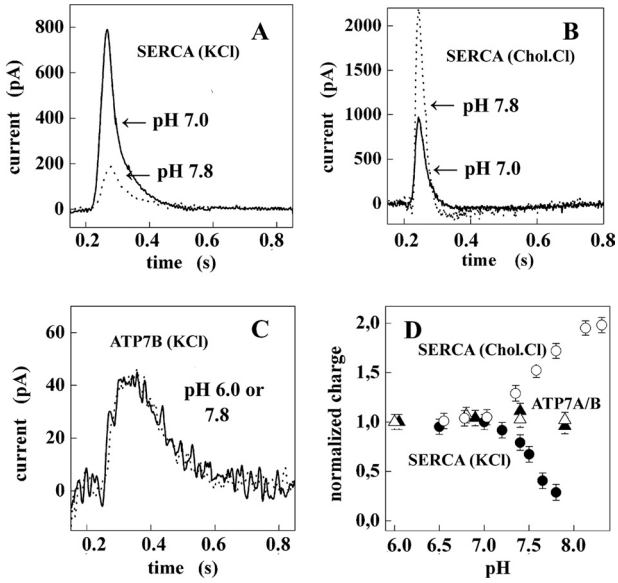

FIGURE 5. **Charge measurements on native SR Ca^{2+} ATPase (SERCA) and recombinant Cu^{+} ATPase (ATP7A and ATP7B).** *A*, current transients were obtained after 100 μM ATP concentration jumps on SERCA in the presence of 10 μM free Ca^{2+} and 100 mM KCl at pH 7 (*solid line*) and 7.8 (*dotted line*). *B*, current transients were obtained after 100 μM ATP concentration jumps on SERCA in the presence of 10 μM free Ca^{2+} and 100 mM choline chloride (*Chol.Cl*) at pH 7 (*solid line*) and 7.8 (*dotted line*). *C*, shown are current transients obtained after 100 μM ATP concentration jumps on ATP7B in the presence of 5 μM $CuCl_2$ and 300 mM KCl at pH 6 (*solid line*) and 7.8 (*dotted line*). *D*, shown is dependence of the normalized charge after 100 μM ATP concentration jumps on pH in the case of ATP7A (△), ATP7B (▲), and SERCA (100 mM KCl, ●; and 100 mM choline chloride, ○). For each protein, the charges are normalized with respect to the value measured at pH 7. S.E. are given by *error bars* in the *lower right panel*.

When ATP is added to ATP7B already activated by copper, formation of phosphoenzyme intermediate is much slower than observed with SERCA and strongly temperature-dependent (Fig. 4*C*). In fact, not only the rate of phosphorylation but (contrary to SERCA) even the steady state level of phosphoenzyme is lower at low temperature. On the other hand, decay of the radioactive phosphoenzyme obtained after a chase with excess nonradioactive ATP shows rather low temperature dependence (Fig. 4*E*). This indicates that higher activation energy is required for initial formation of phosphoenzyme intermediate than for its subsequent processing. *E*P formation and its subsequent decay are faster at alkaline than at acid pH (Fig. 4, *D* and *F*).

Charge Transfer upon the Addition of ATP to Calcium and Copper ATPases—As previously reported (29, 35, 36), the addition of ATP to microsomal vesicles (containing SERCA or ATP7B) adsorbed on a SSM is followed by an electrogenic event recorded as a current transient. The current transient is due to the flow of electrons along the external circuit toward the electrode surface and is required to compensate for the potential difference across the vesicular membrane produced by displacement of positive charge (attributed to vectorial translocation of bound Ca^{2+} or Cu^{+}) in the direction of the SSM electrode after phosphoenzyme intermediate formation by utilization of ATP (29, 36). The electrical current recorded by the SSM method is a measure of the rate of change of the transmembrane potential and is not sensitive to stationary currents. Therefore, only electrogenic steps within the first catalytic cycle are measured, whereas steady state events after the first cycle are not detected.

It is shown in Fig. 5*A* that in experimenting with SERCA, the total net charge decreases as the pH is raised if the main monovalent cation in the reaction mixture is provided by KCl. On the other hand, if the main cation in the reaction mixture is provided by choline chloride, the total net charge displaced increases as the pH is raised (Fig. 5*B*). This suggests that when lack of H^{+} limits H^{+}/Ca^{2+} exchange (*i.e.* alkaline pH), conformational transitions due to alkaline pH render possible K^{+}/Ca^{2+} exchange and neutralization of charge, whereas choline$^{+}/Ca^{2+}$ exchange does not occur.

Net charge displacement is also observed with microsomal vesicles containing recombinant ATP7A or ATP7B (Fig. 5, *C* and *D*), which is attributed to movement of bound Cu^{+} in the direction of the SSM electrode after phosphoenzyme intermediate formation by utilization of ATP (36). Contrary to SERCA, however, net charge transfer by ATP7A or -B is not modified by

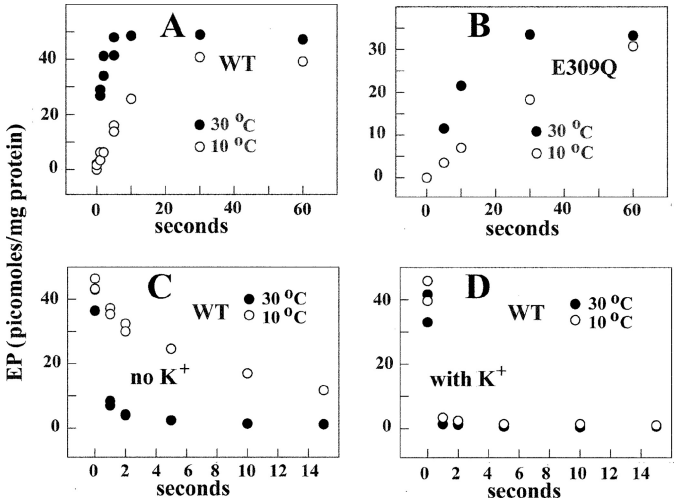

FIGURE 6. **Time course of *E*P formation through utilization of $[^{32}P]P_i$ by WT SERCA (*A*) and E309Q mutant (*B*) and decay (*C* and *D*) of $[^{32}P]$phosphoenzyme after a chase with nonradioactive P_i.** Microsomes derived from COS1 cells expressing SERCA or E309Q mutant were incubated with 50 mM MES, pH 6.0, 20% Me_2SO_4, 10 mM $MgCl_2$, and 2 mM EGTA. The reaction was started by the addition of 50 μM $[^{32}P]P_i$, quenched at different times, and processed for determination of radioactive protein by electrophoretic analysis and detection of radioactivity (see "Experimental Procedures"). For determination of decay, the protein was incubated with 50 μM $[^{32}P]P_i$ as described above at 10 °C for 2 min, and then a 20-fold dilution was obtained with a medium containing 50 mM MES, pH 6.0, 10 mM $MgCl_2$, 2 mM EGTA, and 1 mM nonradioactive P_i at 10 or 30 °C. Serial samples were taken at sequential times for acid quenching and determination of residual radioactive protein by electrophoretic analysis and detection of radioactivity. The experimental points are averages of values obtained in three to four different experiments.

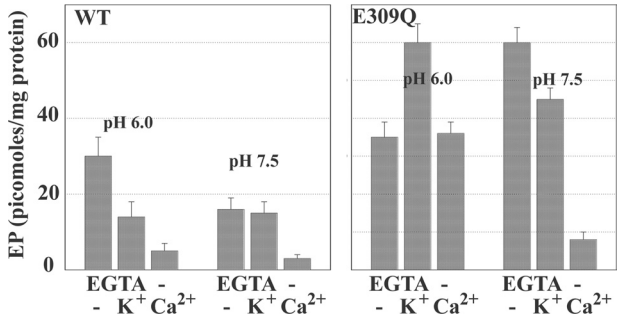

FIGURE 7. **Equilibrium levels of phosphoenzyme obtained through utilization of $[^{32}P]P_i$ by recombinant SERCA and E309Q mutant at acid or alkaline pH.** Effects of K^+ and Ca^{2+} are shown. Microsomes derived from COS1 cells expressing SERCA or mutant (E309Q) protein were diluted (50 μg/ml) in medium containing 50 mM MES (pH 6.0) or HEPES (pH 7.5), 20% Me_2SO_4, and 10 mM $MgCl_2$. 2 mM EGTA, 100 mM KCl, and 1 mM $CaCl_2$ (in the absence of EGTA) were added as indicated in the figure. The reaction was started by the addition of 50 μM $[^{32}P]P_i$ at 30 °C temperature and acid-quenched after 2 min. The quenched samples were processed for determination of radioactive protein by electrophoretic analysis and detection of radioactivity.

raising the pH even though the experiments are performed in the presence of KCl (Fig. 5*C*). This suggests that H^+ exchange upon release of bound cation is specific for SERCA. This is even better demonstrated (Fig. 5*D*) when the pH is stepwise raised in experiments with SERCA in the presence of KCl (●) or choline chloride (○) or ATP7A (△) or ATP7B (▲) in the presence of KCl.

Phosphoenzyme Formation by Utilization of P_i—A very interesting feature of the Ca^{2+} ATPase is its ability to form phosphorylated intermediate by utilization of P_i in the absence of Ca^{2+}. Under the conditions (*i.e.* pH 6, no Ca^{2+} or K^+) originally described (37), this reaction corresponds to E2-P formation by utilization of P_i in the reverse direction of phosphoenzyme cleavage (see Scheme 1). It is noteworthy that, contrary to enzyme activation by Ca^{2+} and phosphorylation by utilization of ATP (Fig. 3), the rates of enzyme phosphorylation with P_i in the absence of Ca^{2+} are significantly temperature-dependent (Fig. 6*A*).

Although utilization of ATP ultimately yields phosphoenzyme steady state levels determined by turnover of the catalytic cycle, experiments with P_i yield equilibrium levels of phosphoenzyme due to the absence of ATP substrate whose potential energy is required to sustain steady state activity. In the P_i reaction, the potential energy is provided by the comparative stability of the protein conformation in the non-phosphorylated *versus* phosphorylated state. Because in the presence of saturating P_i, equilibrium levels of phosphoenzyme are reached within 60 s (Fig. 6), it is possible to determine the dependence of phosphoenzyme equilibrium levels on experimental variables.

For the experiments shown in Figs. 6 and 7, we used both native and recombinant WT SERCA and obtained analogous results. The phosphoenzyme levels shown in the figures were derived from experiments conducted with microsomes obtained from COS1 cells expressing recombinant SERCA (see also Fig. 4*A*) to have a stoichiometric comparison with mutant SERCA (see below). We found that when WT SERCA is used under optimal conditions (*i.e.* pH 6, no Ca^{2+} or K^+), maximal phosphoenzyme levels reach nearly half the stoichiometry of available enzyme, indicating an apparent equilibrium constant of ~1. However, the phosphoenzyme levels are lower if the pH is raised from 6.0 to 7.5 (Fig. 7). Considering that H^+ dissociation favors the E1 over the $2H^+$·E2 postulated in the reaction scheme, it is apparent that E1 has a lower equilibrium constant for the phosphorylation reaction with P_i. Furthermore, in the presence of Ca^{2+} (either at pH 6.0 or 7.5), no significant levels of phosphoenzyme were obtained (Fig. 7). Therefore, the E1·$2Ca^{2+}$ state is unable to utilize P_i for formation of phosphoenzyme. Formation of phosphoenzyme by utilization of P_i is also reduced when KCl (and to a lesser extent NH_4Cl) is present, likely due to enhancement of E2-P cleavage by K^+ coordinated to 711–715 carbonyls and the Glu-732 side chain in the P domain (38).

Functional Characterization of the E309Q SERCA Mutant—Whether the pH dependence of the P_i reaction is regulated specifically by ionization of acidic residues involved in Ca^{2+} binding at the TMBS can be further investigated by characterization of the E309Q SERCA mutant (39). In fact, Glu-309 (Fig. 1) contributes two oxygen atoms to binding of the second Ca^{2+} in the SERCA transmembrane region (12). It was previously reported that a single E309Q mutation interferes with binding of the second Ca^{2+}, rendering the enzyme unable to form phosphorylated intermediate by utilization of ATP in the presence of Ca^{2+} even though still able to bind the first Ca^{2+} (40).

Taking advantage of high yield expression by the use of adenovirus vectors, we are now able to compare the phosphorylation levels of various recombinant proteins. We find that phosphorylation of E309Q mutant protein with P_i occurs with lower

rates but similar temperature dependence to that observed with WT SERCA (Fig. 6, *A* and *B*). The phosphoenzyme formed at pH 6.0 in the absence of Ca^{2+} or K^{+} reached approximately the same levels when the E309Q was used, as compared with WT Ca^{2+} ATPase (Figs. 6 and 7). In addition, no inhibition by Ca^{2+} is observed (39), and a K^{+} effect opposite that observed with WT protein (Fig. 7) suggests that the effect of bound K^{+} in the P domain (38) results in different effects in the E309Q mutant, depending on the pH.

These findings indicate that, at acid pH, the E309Q mutant resides in a state that is still reactive to P_i with a favorable equilibrium constant but, most importantly, is not sensitive to Ca^{2+}. This mutant conformational state is likely produced by a hydrogen bonding pattern that is established at pH 6.0 by the remaining acidic residues at the calcium sites when the Glu-309 acidic chain is absent. When the pH is raised to 7.5, strong inhibition by Ca^{2+} and minor inhibition by K^{+} are observed with the E309Q, in analogy to the WT protein (Fig. 7). However, phosphorylation with P_i reaches a high level (contrary to the effect of high pH on the WT protein), likely related to the absence of Glu-309 acidic chain ionization. Furthermore, a most important difference is the inability of the E309Q mutant to be activated by Ca^{2+} to allow utilization of ATP. This is evidently due to interference by the single E309Q mutation with binding of the second Ca^{2+} that is required for enzyme activation (40). On the other hand, binding of the first calcium (at alkaline pH) is sufficient to interfere with phosphorylation of the E309Q mutant by P_i.

Experiments on Copper ATPase Phosphorylation with P_i—We were not able to obtain significant levels of reverse phosphorylation of ATP7A or -B with P_i when, in analogy to calcium chelation with EGTA, we added BCS to chelate copper in our experiments with ATP7A or -B (Fig. 8). A most interesting result was obtained when the ATP7B Δ5 mutant (in which a large NMBD segment, including the first five copper binding sites, had been deleted) was used. The Δ5 construct yields low expression levels in COS1 cells unless proteasome-mediated degradation is inhibited pharmacologically. However, the Δ5 protein obtained without pharmacologic protection is still able to form *E*P by utilization of ATP and to sustain its hydrolytic cleavage, similarly to WT ATP7B or -A (Fig. 8) (33). Furthermore, *E*P formation by the Δ5 protein shows less temperature dependence than *E*P formation by ATP7B.

Contrary to WT ATP7A and -B, the Δ5 protein undergoes reverse phosphorylation by P_i both in the presence and in the absence of copper (Fig. 8). This demonstrates that the NMBD has a key role in determining orientation and flexibility of the ATP7A/B headpiece domains, with a strong influence on the P domain specific reactivity to ATP or P_i. The lack of copper sensitivity for the P_i reaction is evidently due to removal of the five NMBD copper sites, whereas the copper dependence of the ATP reaction is due to the remaining TMBS copper binding. It is also interesting that ATP utilization by the Δ5 protein yields negligible alkali stable phosphorylation (Fig. 8*A*). This may be partly due to deletion of some of the serine residues undergoing phosphorylation (Fig. 1) but also to interference by the Δ5 deletion with docking of protein kinase C.

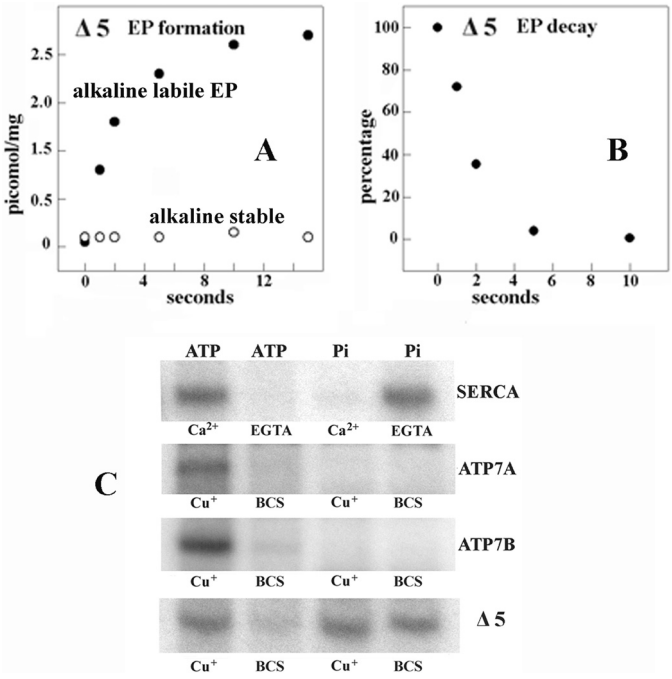

FIGURE 8. **Functional behavior of Δ5 ATP7B (large NMBD segment deleted).** *A* and *B*, formation of [γ-^{32}P]phosphoenzyme after [γ-^{32}P]ATP utilization by Δ5 ATP7B and decay of [γ-^{32}P]phosphoenzyme after a chase with excess nonradioactive ATP. The experiments were performed at pH 6.0 and 10 °C temperature as described in the legend to Fig. 4. The low phosphoenzyme levels are due to low concentration of expressed protein in the microsomes of the infected COS-1 cells. *C*, electrophoretic demonstration of phosphoenzyme formation through utilization of [γ-^{32}P]ATP or [^{32}P]P_i by SERCA, ATP7A, ATP7B, and Δ5 ATP7B is shown. Microsomes derived from COS1 cells expressing SERCA were incubated with 50 μM [γ-^{32}P]ATP for 5 s at 30 °C in a reaction mixture containing 50 mM MES (pH 6.0), 3 mM $MgCl_2$, 100 mM KCl, and 10 μM $CaCl_2$ or 2 mM EGTA as indicated. Microsomes derived from COS1 cells expressing ATP7A, ATP7B, or Δ5 ATP7B mutant protein were incubated with 50 μM [γ-^{32}P]ATP for 5 s at 30 °C in a reaction mixture containing 50 mM MES, pH 6.0, 300 mM KCl, 10 mM DTT, 3 mM $MgCl_2$, and 5 μM $CuCl_2$ or 2 mM BCS as indicated. Alternatively, microsomes derived from COS1 cells expressing SERCA were incubated with 50 μM [^{32}P]P_i for 2 min at 30 °C in a reaction mixture containing 50 mM MES, pH 6.0, 10 mM $MgCl_2$, 20% Me_2SO_4, and 1 mM $CaCl_2$ or 2 mM EGTA as indicated. Microsomes derived from COS1 cells expressing ATP7A, ATP7B, or Δ5 ATP7B mutant protein were incubated with 50 μM [γ-^{32}P]P_i for 2 min at 30 °C in a reaction mixture containing 50 mM MES (pH 6.0), 10 mM DTT, 10 mM $MgCl_2$, 20% Me_2SO_4, and 5 μM $CuCl_2$ or 2 mM BCS as indicated. The reactions were acid-quenched, and the samples were processed for determination of radioactive protein by electrophoretic analysis and detection of radioactivity. It is noteworthy that no kinase-mediated Ser/Thr phosphorylation was noted when P_i rather than ATP was used as a substrate.

DISCUSSION

The experiments reported above offer a comparative characterization of the SERCA and ATP7A/B mechanisms, which we relate here to known structural features (available in greater detail for SERCA) and may also be helpful to explain further structural information on WT and mutant proteins as it will be obtained.

SERCA crystal structures show that the headpiece domains are widely separated in the transition from E2 to E1·2Ca^{2+} and approximate again upon nucleotide binding and formation of E1-P (12, 41, 42). Bending and rotation of the headpieces occur in conjunction with related displacement of membrane-bound segments. Our experiments demonstrate that the rate of SERCA activation by Ca^{2+} is rate-limiting for phosphorylation by ATP. The activation rate is slower at acid than at alkaline pH

but is affected very little by raising the temperature (Fig. 3). This indicates that, in the native membrane environment, the rate of $2H^{+}$·E2 transition to E1 has rather low dependence on activation energy.

On the other hand, the high temperature dependence of phosphoenzyme decay (Fig. 3) and reverse phosphorylation by P_i (Fig. 6) indicate that conformational constraints limiting related transitions are sensitive to temperature-dependent activation energy in addition to being driven by phosphorylation-related potential energy as E1-P converts to E2-P. Diverse conformations of intermediate states (or analogs thereof) have been revealed by crystallography, indicating structural features involved in isomerization of E1-P to E2-P, cleavage of P_i, and return of E2 to E1 (8, 9). From the functional point of view, sequential transitions of these intermediate conformations yield vectorial translocation and release of bound Ca^{2+} in exchange for luminal H^{+} (29, 43–45).

Relevance of acidic residues was first indicated by the pH dependence of Ca^{2+} binding to SERCA in the absence of ATP, with affinity increasing from pH 6 to 8 (46, 47). Mutational analysis (39, 40, 48) and high resolution crystallography (12) then demonstrated that, within the membrane-bound region, Ca^{2+} binding at site I (Fig. 9) involves the side chain oxygen atoms of Asn-768, Glu-771 (M5), Thr-799, Asp-800 (M6), and Glu-908 (M8), and two water molecules. Ca^{2+} binding at site II (Fig. 9) involves three main chain carbonyls derived from partly unwound M4 helix, Asn-796 and Asp-800 side chain oxygen atoms (M6), and two capping oxygen atoms from Glu-309 (M4). A stable conformation (E1) is thereby obtained due to high affinity Ca^{2+} binding.

In the absence of Ca^{2+}, a different conformation (E2) is acquired by SERCA. For structural studies by crystallization, the E2 conformation has been stabilized by binding of inhibitors such as thapsigargin (42) and dibutyldihydroxybenzene (44). However, it is important to consider that in the native membrane and in the absence of inhibitors, orientation and protonation of acidic chains as well as related hydrogen bonding patterns provide conformational stability for the Ca^{2+}-free state (Fig. 9 as demonstrated in Obara *et al.* (44). Molecular dynamics calculations yield p*K* values allowing protonation (44, 49, 50) of three or four acidic residues (Glu-309, Glu-771, Glu-908, and Asp-800) and permitting hydrogen bonding that would be optimal at pH 6. On the other hand, in the absence of Ca^{2+}, alkaline pH interferes with hydrogen bonding at the calcium site and consequently yields conformational destabilization (44, 50). Experiments with fluorescent styryl dyes and analysis of pH jump-induced relaxation process have shown a conformational transition of the empty E2-P as the pH is raised, attributed to a reversible inactivated state (51).

The experiments reported here indicate that the acidic residues in the transmembrane calcium binding domain region sustain an important role in conformational transitions pertinent to enzyme activation and transduction mechanism. In fact, the faster rate of SERCA activation observed when Ca^{2+} and ATP are added to SERCA previously exposed to alkaline pH (Fig. 3) demonstrates that dissociation of H^{+} from acidic residues accelerates the transition from E2 to E1. Furthermore, after ATP utilization at acid and to some extent at neutral pH,

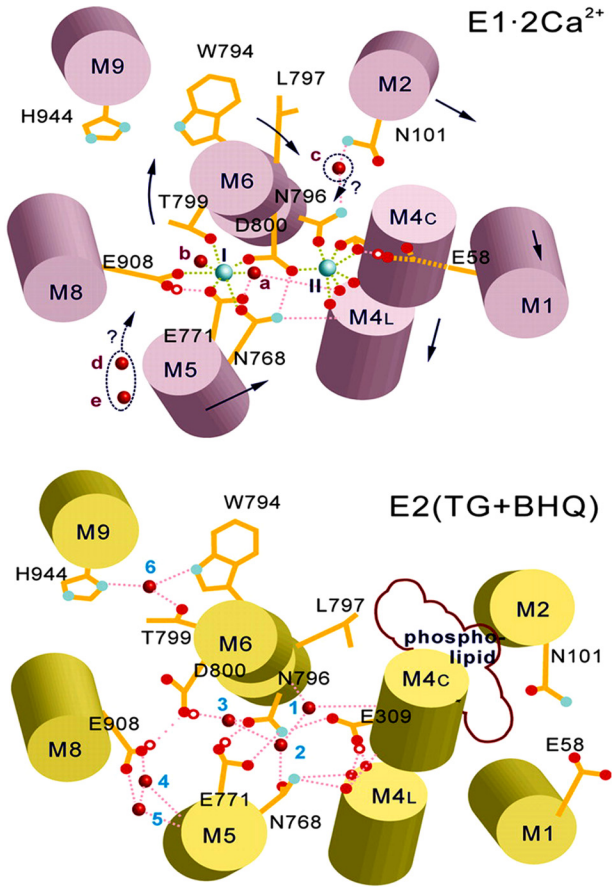

FIGURE 9. **Diagram of the SERCA Ca^{2+} binding sites in the E1·2Ca^{2+} and in the E2 state stabilized by thapsigargin (*TG*) and dibutyldihydroxybenzene (BHQ) (44) based on crystallography (12, 42) and continuum of electrostatic calculations.** The *larger cyan spheres in the upper diagram* represent bound Ca^{2+} (*I* and *II*), and the *small red spheres* represent water. *Small red circles* represent bound protons, *dotted pink lines* represent hydrogen bonds, and *green dotted lines* represent Ca^{2+} coordination. The *arrows* indicate possible movements upon state transition. Data are derived from Obara *et al.* (44).

protonation of acidic residues occurs as a consequence of Ca^{2+}/H^{+} exchange upon Ca^{2+} release from E2-P (43, 45), as also shown by charge movement observed in single cycle experiments (Fig. 5). At alkaline pH, Ca^{2+}/H^{+} exchange and protonation of acidic residues occurs less or not at all, whereas Ca^{2+} may exchange with K^{+} as long as the luminal Ca^{2+} concentration is low (Fig. 5; see also Musgaard *et al.* (50) or may remain bound to the transport sites when the luminal Ca^{2+} concentration rises. Alteration of Ca^{2+}/H^{+} exchange results in low transport efficiency.

It is noteworthy that although pH and concentrations of various ligands may be optimized to favor crystallization or biochemical events under experimental conditions, pH and concentrations of ligands (except Ca^{2+}) do not change under physiological conditions. Protonation and ionization are then determined by changes in pK as acidic residues of the pathway face the lumenal or the cytosolic surface of the membrane (52). Therefore, Ca^{2+}/H^{+} exchange and protonation of acidic residues sustain an important role in conformational transitions and selective ion movements within the transport cycle. In analogy to the calcium-occluded state, a proton-occluded state has been proposed (53) based on structural studies of E2-AlF_4^-

crystals. We conclude that the transmembrane Ca^{2+} binding region, in addition to its linkage to phosphorylation of the cytosolic head for energy transduction, behaves as a H^{+}-gated Ca^{2+} pathway for efficient translocation of Ca^{2+}. A requirement for specific conformational transitions of this pathway was demonstrated by interference with the neighboring Cys-876–Cys-888 disulfide bond, which produces inhibition of Ca^{2+} transport, whereas full ATPase activity is retained (54).

Functional characterization of the E309Q mutant reveals interesting details on the conformational effects of protonated acidic residues at the calcium sites. We see that the mutant protein retains the ability to form phosphoenzyme by utilization of P_i at pH 6.0 (Figs. 6 and 7), as expected of the E2 state. Yet, using the proteolytic digestion analysis originally introduced by (55), we previously demonstrated that the E309Q mutation favors an A domain position similar to that of E1 (32) rather than E2, even in the absence of Ca^{2+}. This does not mean that the entire conformation is E1-like, as shown by its reactivity to P_i (Fig. 7). It is apparent that this peculiar conformation of the mutant is stabilized by a hydrogen bonding pattern established by the remaining residues (Glu-771, Asp-800, and Glu-908) at acid pH. Therefore, in WT SERCA, the E2 state must be maintained specifically by the protonated Glu-309 residue in a rather strained conformation and, if the Glu-309 H^{+} is dissociated by raising the pH, the enzyme shifts to the E1 state. If the residual hydrogen bonding pattern of the E309Q protein is interfered with by raising the pH to 7.5, the mutant acquires Ca^{2+} sensitivity analogous to that of WT protein, with regard to inhibition of reverse phosphorylation with P_i (Fig. 7). However, even at alkaline pH, ATP cannot be utilized by the E309Q mutant upon the addition of Ca^{2+} as the second Ca^{2+} is not bound by the mutant at any pH. It is apparent that, in the WT protein, the acidic function of Glu-309 has conformational implications in the absence as well as in the presence of Ca^{2+}. It is certainly involved in the E_2 to E_1 transition, binding the second Ca^{2+} required for catalytic activation, and occlusion of the bound Ca^{2+} upon formation of phosphorylated intermediate (56).

In comparative experiments we found that, contrary to SERCA, the rate of phosphoenzyme formation by ATP7B is highly temperature-dependent (Fig. 4*C*), whereas the rate of phosphoenzyme decay has a low temperature dependence (Fig. 4*E*). For this reason, the steady state levels of phosphoenzyme are lower at low temperature for ATP7B, whereas they are higher for SERCA. This suggests that overcoming conformational constraints, related to headpiece interactions with the NMBD (which is not present in SERCA), requires significant energy of activation to reach the phosphorylated state. These constraints pose a significant limit to initiation of the cycle as compared with SERCA, as also demonstrated by the slower kinetics of ATP-dependent charge transfer (Fig. 5).

Another interesting phenomenon is the lack of reverse ATP7B phosphorylation with P_i, suggesting that copper chelation with BCS and dissociation from the NMBD sites favors interactions of the NMBD chain with the enzyme headpiece that interfere with the phosphorylation reaction. In fact, deletion of a large segment of the NMBD allows the deleted protein (Δ5) to undergo phosphorylation by P_i (Fig. 8). This is in agreement with previous studies with *Thermotoga maritima* (CopA) copper ATPase (57), where the NMBD is much shorter (a single metal binding site) than that of ATP7B (six metal binding sites), and the enzyme yields high phosphorylation levels with P_i. Furthermore, the ability of the Δ5 protein to utilize ATP (Fig. 8) suggests that the deleted NMBD segment (five of six copper sites) is not necessary for catalytic activity. Its function may be related to favoring ATP7A/B interaction with other proteins involved in cellular copper homeostasis.

Finally, contrary to SERCA, net charge transfer by ATP7A or -B is not altered by raising the pH and is not reduced by K^{+} (Fig. 5). This indicates that cation/H^{+} exchange at the transport site does not play a role in copper release. In fact, structural studies of *Legionella pneumophila* (CopA) copper ATPase (58) do not reveal obvious involvement of acidic chains in the release phase of copper transport. Other specific mechanisms may be involved in promoting copper release from intramembrane sites of the copper ATPase, such as revealed by experiments on the Met-672–Pro-707 lumenal loop (59).

In conclusion, we find that comparative experiments with mammalian copper ATPases demonstrate distinctive mechanistic features whose knowledge complements the limited information as yet available on high resolution structure for this enzyme. Conformational constraints limiting the rate of initial phosphoenzyme intermediate formation by utilization of ATP and sensitivity to temperature-dependent activation energy are evidently related to interactions of the headpiece domains with the NMBD extension, which is not present in SERCA. These interactions are also reflected by the reverse phosphorylation reaction with P_i. On the other hand, the low temperature dependence of phosphoenzyme turnover and the lack of H^{+} exchange suggest that greater conformational changes are sustained in concomitance with phosphorylation by ATP and comparatively less for copper release from the phosphoenzyme.

Acknowledgment—G. I. is deeply indebted to Professor Chikashi Toyoshima for many suggestions and comments.

REFERENCES

1. Albers, R. W. (1967) Biochemical aspects of active transport. *Annu. Rev. Biochem.* **36,** 727–756
2. de Meis, L., and Vianna, A. L. (1979) Energy interconversion by the Ca^{2+}-dependent ATPase of the sarcoplasmic reticulum. *Annu. Rev. Biochem.* **48,** 275–292
3. Post, R. L., Hegyvary, C., and Kume, S. (1972) Activation by adenosine triphosphate in the phosphorylation kinetics of sodium and potassium ion transport adenosine triphosphatase. *J. Biol. Chem.* **247,** 6530–6540
4. Brini, M., and Carafoli, E. (2009) Calcium pumps in health and disease. *Physiol. Rev.* **89,** 1341–1378
5. MacLennan, D. H., Brandl, C. J., Korczak, B., and Green, N. M. (1985) Amino-acid sequence of a Ca^{2+} + Mg^{2+}-dependent ATPase from rabbit muscle sarcoplasmic reticulum, deduced from its complementary DNA sequence. *Nature* **316,** 696–700
6. Lutsenko, S., and Kaplan, J. H. (1995) Organization of P-type ATPases. Significance of structural diversity. *Biochemistry* **34,** 15607–15613
7. Pedersen, P. L., and Carafoli, E. (1987) Ion motive ATPases. II. Energy coupling and work output. *Trends Biochem. Sci.* **12,** 186–189
8. Toyoshima, C., and Inesi, G. (2004) Structural basis of ion pumping by Ca^{2+}-ATPase of the sarcoplasmic reticulum. *Annu. Rev. Biochem.* **73,** 269–292

9. Møller, J. V., Olesen, C., Winther, A. M., and Nissen, P. (2010) The sarcoplasmic Ca^{2+}-ATPase. Design of a perfect chemi-osmotic pump. *Q. Rev. Biophys.* **43,** 501–566
10. Andersen, J. P., and Vilsen, B. (1995) Structure-function relationships of cation translocation by Ca^{2+}- and Na^{+}, K^{+}-ATPases studied by site-directed mutagenesis. *FEBS Lett.* **359,** 101–106
11. Inesi, G., Kurzmack, M., Coan, C., and Lewis, D. E. (1980) Cooperative calcium binding and ATPase activation in sarcoplasmic reticulum vesicles. *J. Biol. Chem.* **255,** 3025–3031
12. Toyoshima, C., Nakasako, M., Nomura, H., and Ogawa, H. (2000) Crystal structure of the calcium pump of sarcoplasmic reticulum at 2.6 Å resolution. *Nature* **405,** 647–655
13. Dierick, H. A., Ambrosini, L., Spencer, J., Glover, T. W., and Mercer, J. F. (1995) Molecular structure of the Menkes disease gene (ATP7A). *Genomics* **28,** 462–469
14. Tümer, Z., Vural, B., Tønnesen, T., Chelly, J., Monaco, A. P., and Horn, N. (1995) Characterization of the exon structure of the Menkes disease gene using vectorette PCR. *Genomics* **26,** 437–442
15. Petrukhin, K., Lutsenko, S., Chernov, I., Ross, B. M., Kaplan, J. H., and Gilliam, T. C. (1994) Characterization of the Wilson disease gene encoding a P-type copper transporting ATPase. Genomic organization, alternative splicing, and structure/function predictions. *Hum. Mol. Genet.* **3,** 1647–1656
16. Mercer, J. F., Barnes, N., Stevenson, J., Strausak, D., and Llanos, R. M. (2003) Copper-induced trafficking of the Cu-ATPases. A key mechanism for copper homeostasis. *Biometals* **16,** 175–184
17. Voskoboinik, I., Greenough, M., La Fontaine, S., Mercer, J. F., and Camakaris, J. (2001) Functional studies on the Wilson copper P-type ATPase and toxic milk mouse mutant. *Biochem. Biophys. Res. Commun.* **281,** 966–970
18. Tsivkovskii, R., Purnat, T., and Lutsenko, S. (2004) in *Handbook of ATPases: Biochemistry, Cell Biology, Pathophysiology* (Futai, M., Kaplan, J. H., and Wada, Y., eds) pp. 99–158, Wiley-VCH, Weinheim, Germany
19. Lutsenko, S., Barnes, N. L., Bartee, M. Y., and Dmitriev, O. Y. (2007) Function and regulation of human copper-transporting ATPases. *Physiol. Rev.* **87,** 1011–1046
20. Argüello, J. M., González-Guerrero, M., and Raimunda, D. (2011) Bacterial transition metal P_{1B}-ATPases. Transport mechanism and roles in virulence. *Biochemistry* **50,** 9940–9949
21. Pilankatta, R., Lewis, D., Adams, C. M., and Inesi, G. (2009) High yield heterologous expression of wild-type and mutant Cu^{+}-ATPase (ATP7B, Wilson disease protein) for functional characterization of catalytic activity and serine residues undergoing copper-dependent phosphorylation. *J. Biol. Chem.* **284,** 21307–21316
22. Eletr, S., and Inesi, G. (1972) Phase changes in the lipid moieties of sarcoplasmic reticulum membranes induced by temperature and protein conformational changes. *Biochim. Biophys. Acta* **290,** 178–185
23. Laemmli, U. K. (1970) Cleavage of structural proteins during the assembly of the head of bacteriophage T4. *Nature* **227,** 680–685
24. Weber, K., and Osborn, M. (1969) The reliability of molecular weight determinations by dodecyl sulfate-polyacrylamide gel electrophoresis. *J. Biol. Chem.* **244,** 4406–4412
25. Pintschovius, J., and Fendler, K. (1999) Charge translocation by the Na^{+}/K^{+}-ATPase investigated on solid supported membranes. Rapid solution exchange with a new technique. *Biophys. J.* **76,** 814–826
26. Schulz, P., Garcia-Celma, J. J., and Fendler, K. (2008) SSM-based electrophysiology. *Methods* **46,** 97–103
27. Tadini-Buoninsegni, F., Bartolommei, G., Moncelli, M. R., and Fendler, K. (2008) Charge transfer in P-type ATPases investigated on planar membranes. *Arch. Biochem. Biophys.* **476,** 75–86
28. Patton, C., Thompson, S., and Epel, D. (2004) Some precautions in using chelators to buffer metals in biological solutions. *Cell Calcium* **35,** 427–431
29. Tadini-Buoninsegni, F., Bartolommei, G., Moncelli, M. R., Guidelli, R., and Inesi, G. (2006) Pre-steady state electrogenic events of Ca^{2+}/H^{+} exchange and transport by the Ca^{2+}-ATPase. *J. Biol. Chem.* **281,** 37720–37727
30. Scarpa, A., Baldassare, J., and Inesi, G. (1972) The effect of calcium ionophores on fragmented sarcoplasmic reticulum. *J. Gen. Physiol.* **60,** 735–749
31. Inesi, G., and Watanabe, S. (1967) Temperature dependence of ATP hydrolysis and calcium uptake by fragmented sarcoplasmic membranes. *Arch. Biochem. Biophys.* **121,** 665–671
32. Inesi, G., Lewis, D., Toyoshima, C., Hirata, A., and de Meis, L. (2008) Conformational fluctuations of the Ca^{2+}-ATPase in the native membrane environment. Effects of pH, temperature, catalytic substrates, and thapsigargin. *J. Biol. Chem.* **283,** 1189–1196
33. Pilankatta, R., Lewis, D., and Inesi, G. (2011) Involvement of protein kinase D in expression and trafficking of ATP7B (copper ATPase). *J. Biol. Chem.* **286,** 7389–7396
34. Liu, Y., Pilankatta, R., Hatori, Y., Lewis, D., and Inesi, G. (2010) Comparative features of copper ATPases ATP7A and ATP7B heterologously expressed in COS-1 cells. *Biochemistry* **49,** 10006–10012
35. Tadini Buoninsegni, F., Bartolommei, G., Moncelli, M. R., Inesi, G., and Guidelli, R. (2004) Time-resolved charge translocation by sarcoplasmic reticulum Ca-ATPase measured on a solid supported membrane. *Biophys. J.* **86,** 3671–3686
36. Tadini-Buoninsegni, F., Bartolommei, G., Moncelli, M. R., Pilankatta, R., Lewis, D., and Inesi, G. (2010) ATP-dependent charge movement in ATP7B Cu^{+}-ATPase is demonstrated by pre-steady state electrical measurements. *FEBS Lett.* **584,** 4619–4622
37. Masuda, H., and de Meis, L. (1973) Phosphorylation of the sarcoplasmic reticulum membrane by orthophosphate. Inhibition by calcium ions. *Biochemistry* **12,** 4581–4585
38. Sørensen, T. L., Clausen, J. D., Jensen, A. M., Vilsen, B., Møller, J. V., Andersen, J. P., and Nissen, P. (2004) Localization of a K^{+}-binding site involved in dephosphorylation of the sarcoplasmic reticulum Ca^{2+}-ATPase. *J. Biol. Chem.* **279,** 46355–46358
39. Clarke, D. M., Loo, T. W., Inesi, G., and MacLennan, D. H. (1989) Location of high affinity Ca^{2+}-binding sites within the predicted transmembrane domain of the sarcoplasmic reticulum Ca^{2+}-ATPase. *Nature* **339,** 476–478
40. Strock, C., Cavagna, M., Peiffer, W. E., Sumbilla, C., Lewis, D., and Inesi, G. (1998) Direct demonstration of Ca^{2+} binding defects in sarco-endoplasmic reticulum Ca^{2+} ATPase mutants overexpressed in COS-1 cells transfected with adenovirus vectors. *J. Biol. Chem.* **273,** 15104–15109
41. Sørensen, T. L., Møller, J. V., and Nissen, P. (2004) Phosphoryl transfer and calcium ion occlusion in the calcium pump. *Science* **304,** 1672–1675
42. Toyoshima, C., and Nomura, H. (2002) Structural changes in the calcium pump accompanying the dissociation of calcium. *Nature* **418,** 605–611
43. Yu, X., Carroll, S., Rigaud, J. L., and Inesi, G. (1993) H^{+} countertransport and electrogenicity of the sarcoplasmic reticulum Ca^{2+} pump in reconstituted proteoliposomes. *Biophys. J.* **64,** 1232–1242
44. Obara, K., Miyashita, N., Xu, C., Toyoshima, I., Sugita, Y., Inesi, G., and Toyoshima, C. (2005) Structural role of countertransport revealed in Ca^{2+} pump crystal structure in the absence of Ca^{2+}. *Proc. Natl. Acad. Sci. U.S.A.* **102,** 14489–14496
45. Levy, D., Seigneuret, M., Bluzat, A., and Rigaud, J. L. (1990) Evidence for proton countertransport by the sarcoplasmic reticulum Ca^{2+}-ATPase during calcium transport in reconstituted proteoliposomes with low ionic permeability. *J. Biol. Chem.* **265,** 19524–19534
46. Forge, V., Mintz, E., and Guillain, F. (1993) Ca^{2+} binding to sarcoplasmic reticulum ATPase revisited. I. Mechanism of affinity and cooperativity modulation by H^{+} and Mg^{2+}. *J. Biol. Chem.* **268,** 10953–10960
47. Watanabe, T., Lewis, D., Nakamoto, R., Kurzmack, M., Fronticelli, C., and Inesi, G. (1981) Modulation of calcium binding in sarcoplasmic reticulum adenosine triphosphatase. *Biochemistry* **20,** 6617–6625
48. Andersen, J. P., and Vilsen, B. (1998) Structure-function relationships of the calcium binding sites of the sarcoplasmic reticulum Ca^{2+}-ATPase. *Acta Physiol. Scand. Suppl.* **643,** 45–54
49. Andersson, J., Hauser, K., Karjalainen, E. L., and Barth, A. (2008) Protonation and hydrogen bonding of Ca^{2+} site residues in the E_2P phosphoenzyme intermediate of sarcoplasmic reticulum Ca^{2+}-ATPase studied by a combination of infrared spectroscopy and electrostatic calculations. *Biophys. J.* **94,** 600–611
50. Musgaard, M., Thøgersen, L., and Schiøtt, B. (2011) Protonation states of important acidic residues in the central Ca^{2+} ion binding sites of the Ca^{2+}-

ATPase. A molecular modeling study. *Biochemistry* **50,** 11109–11120
51. Fibich, A., and Apell, H. J. (2011) Kinetics of luminal proton binding to the SR Ca-ATPase. *Biophys. J.* **101,** 1896–1904
52. Yu, X., Hao, L., and Inesi, G. (1994) A p*K* change of acidic residues contributes to cation countertransport in the Ca-ATPase of sarcoplasmic reticulum. Role of H^+ in Ca^{2+}-ATPase countertransport. *J. Biol. Chem.* **269,** 16656–16661
53. Olesen, C., Sørensen, T. L., Nielsen, R. C., Møller, J. V., and Nissen, P. (2004) Dephosphorylation of the calcium pump coupled to counterion occlusion. *Science* **306,** 2251–2255
54. Daiho, T., Yamasaki, K., Saino, T., Kamidochi, M., Satoh, K., Iizuka, H., and Suzuki, H. (2001) Mutations of either or both Cys-876 and Cys-888 residues of sarcoplasmic reticulum Ca^{2+}-ATPase result in a complete loss of Ca^{2+} transport activity without a loss of Ca^{2+}-dependent ATPase activity. Role of the Cys-876–Cys-888 disulfide bond. *J. Biol. Chem.* **276,** 32771–32778
55. Danko, S., Yamasaki, K., Daiho, T., Suzuki, H., and Toyoshima, C. (2001) Organization of cytoplasmic domains of sarcoplasmic reticulum Ca^{2+}-ATPase in E_1P and E_1ATP states. A limited proteolysis study. *FEBS Lett.* **505,** 129–135
56. Inesi, G., Ma, H., Lewis, D., and Xu, C. (2004) Ca^{2+} Occlusion and gating function of Glu-309 in the ADP-fluoroaluminate analog of the Ca^{2+}-ATPase phosphoenzyme intermediate. *J. Biol. Chem.* **279,** 31629–31637
57. Hatori, Y., Hirata, A., Toyoshima, C., Lewis, D., Pilankatta, R., and Inesi, G. (2008) Intermediate phosphorylation reactions in the mechanism of ATP utilization by the copper ATPase (CopA) of *Thermotoga maritima*. *J. Biol. Chem.* **283,** 22541–22549
58. Gourdon, P., Liu, X. Y., Skjørringe, T., Morth, J. P., Møller, L. B., Pedersen, B. P., and Nissen, P. (2011) Crystal structure of a copper-transporting PIB-type ATPase. *Nature* **475,** 59–64
59. Barry, A. N., Otoikhian, A., Bhatt, S., Shinde, U., Tsivkovskii, R., Blackburn, N. J., and Lutsenko, S. (2011) The lumenal loop Met-672–Pro-707 of copper-transporting ATPase ATP7A binds metals and facilitates copper release from the intramembrane sites. *J. Biol. Chem.* **286,** 26585–26594